

# The structure of the Hoyle state and its $2^+$ partner state in $^{12}\text{C}$

Moshe Gai for the UConn-Yale-TUNL-Weizmann-PTB-UCL collaboration

Laboratory for Nuclear Science at Avery Point

University of Connecticut, 1084 Shennecossett Rd, Groton, CT 06340-6097, USA

**Abstract.** We have measured the  $^{12}\text{C}(\gamma, 3\alpha)$  reaction with an Optical Time Projection Chamber (O-TPC) detector operating with the  $\text{CO}_2(80\%) + \text{N}_2(20\%)$  gas mixture and gamma-ray beams from the HIγS facility of the TUNL at Duke. We measured complete angular distributions (between 9.1 - 10.7 MeV) from which we determine the cross section yield curve and  $E1 - E2$  relative phases leading to an unambiguous identification of the second  $2^+$  state in  $^{12}\text{C}$  at 10.03(11) MeV. The observed spectrum of  $^{12}\text{C}$  below 12 MeV including the  $2_2^+$  state observed in this work resembles the rotation-vibration spectrum predicted for a triangular shape oblate spinning top in which the Hoyle state is the first vibrational breathing mode of the triangular three alpha-particle system. We also observed a hint of the  $2_3^+$  state which is predicted by the U(7) model as a member of the  $1^-$  bending mode band, but the existence of this  $2_3^+$  is yet to be confirmed. The predicted rotation-vibration spectrum of a triangular shape oblate spinning top (with a  $\mathcal{D}_{3h}$  symmetry) allows us to compare the moment of inertia of the predicted Hoyle rotational band to the ground state rotational band and in this way extract the (large) rms radius of the Hoyle state of 3.22(8) fm. We compare the deduced rms radius with recent ab-initio theories and cluster models as well as the radius extracted from  $^{12}\text{C}(p, p')$  data.

## 1 Introduction

The second  $0^+$  state at 7.654 MeV in  $^{12}\text{C}$  that was first predicted (in 1953) by Hoyle [1] plays a central role in nuclear physics. Ever since Brink suggested that the Hoyle state is a very extended object with the structure of three alpha-particles arranged in a linear chain [2] many theoretical models were developed to describe the Hoyle state and the structure of  $^{12}\text{C}$ . One of the issues of great current interest is whether the Hoyle state is an extended object with an rms radius considerably larger than the ground state of  $^{12}\text{C}$ . Indeed, clusterization is thought to occur in nuclear matter with low density (e.g. one third of the central density of nuclei). As such for an extended Hoyle state clusterization can occur throughout the nucleus and not as typically found on the surface of nuclei. In this paper we deduce the rms radius of the Hoyle state from the moment of inertia of the rotational band built on top of the Hoyle state and we conclude that the rms radius of the Hoyle state is considerably (35%) larger than the ground state.

A number of models have been proposed to describe the structure of  $^{12}\text{C}$  including a group theoretical U(7) model with a  $\mathcal{D}_{3h}$  symmetry [3], a microscopic Fermionic Molecular Dynamic (FMD) model [4] together with "BEC-like" cluster model [5], ab-initio no core shell model [6,7], and ab-initio lattice Effective Field Theory (EFT) [8,9]. It is shown by the ab-initio no core shell model calculations that the Hoyle state can only be described by a  $10 \hbar\omega$  shell model space [7], suggesting that it is an extended alpha-clustering configuration.

Current models differ on the shape of the Hoyle state. In the U(7) model and the FMD model the Hoyle state is predicted to be an oblate triangular three alpha-particle configuration. In the frame of the EFT theory [9] the Hoyle state is primarily of the bent-arm chain (or obtuse triangu-

lar) shape. Both ab-initio no core shell model calculations [7] and EFT calculations [9] predict the Hoyle state to be of deformed prolate shape. In addition while the FMD model predicts an rms radius of the Hoyle state (3.48 fm) that is  $\sqrt{2}$  larger than the ground state (2.39 fm) [4], calculations in the frame of the ab-initio EFT theory [9] predicts an rms radius (2.4 fm) equal (within the predicted error bar) to the rms radius of the ground state of  $^{12}\text{C}$  and the ab-initio no core shell model calculations [7] predict an rms radius (2.93 fm) that is only 22% larger than the ground state of  $^{12}\text{C}$ .

The three alpha-particle structure of  $^{12}\text{C}$  naturally leads to models that utilize triangular geometry [3,4,8,9]. Such triangular systems are ubiquitous in physics including the  $X_3$  molecular system [10], and the three quark system [11, 12] and their spectrum resemble the one predicted by the oblate spinning top with a  $\mathcal{D}_{3h}$  symmetry [10,11]. The rotation-vibration spectrum predicted for the triangular three alpha-particle oblate spinning top appears to be a very useful phenomenological framework to discuss the (rotation-vibration) spectrum of the three alpha-particle system of  $^{12}\text{C}$  [3]. It is phenomenological schematic model (e.g. it treats bound and quasi-bound states in the same framework) that serves as a useful guide in which to discuss the essential degrees of freedom of the three alpha-particle system.

For example in the U(7) model the Hoyle state is predicted to be the first vibrational breathing mode of the (oblate) deformed state on top of which a rotational band is predicted which is very similar to the ground state rotational band with the same triangular geometry. In contrast, for example the FMD model [4] and the "BEC-like" cluster models [5] do not predict the  $2_2^+$  to be a member of a rotational band. The EFT calculations [9] on the other

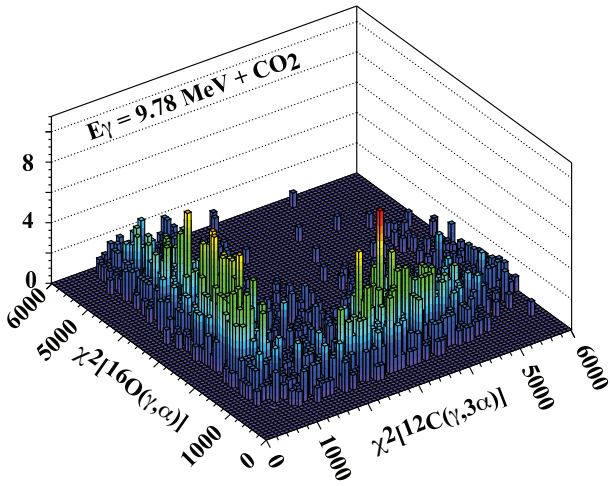


**Fig. 1.** Event identification using the  $\chi^2$  evaluated for each event using the line shape of the  $^{16}\text{O}(\gamma, \alpha)$  and the  $^{12}\text{C}(\gamma, 3\alpha)$  dissociation reactions.

hand predict a Hoyle rotational band [9]. The  $1^-$  state at 10.84 MeV is predicted by the U(7) model to be the bending mode of the three alpha-particle system with a rotational band that includes the  $1^-$  and almost degenerate  $2^+$  and  $2^-$  states. Thus this U(7) model also predicts two new  $2^+$  states below 12 MeV in  $^{12}\text{C}$  beyond the ground state  $2^+$ .

## 2 Measurement of the $^{12}\text{C}(\gamma, 3\alpha)$ reaction

The current measurement of the  $^{12}\text{C}(\gamma, 3\alpha)$  reaction was performed at the HIγS facility that produces an intense, nearly monoenergetic gamma-ray beam by Compton back-scattering photons from a free-electron laser [13]. Beam energy spreads of 300 - 350 keV were measured at beam energies between 9.1 and 10.7 MeV, with on-target intensities of  $\approx 2 \times 10^8 \gamma/\text{sec}$ . The beam intensity was measured by detecting neutrons from the  $d(\gamma, n)p$  reaction using a  $D_2O$  target, cross-calibrated against a large NaI(Tl) detector. The energy profile of the beam was measured using a large HPGe detector, and the spectra were unfolded using a Monte Carlo technique [14, 15]. The alignment of the detector with respect to the beam was achieved using a gamma camera and lead absorbers placed in the front and back of the detector [16] as discussed in [17].

An optical-readout time projection chamber (O-TPC) operating at 100 torr with the gas mixture of  $CO_2(80\%) + N_2(20\%)$  described in [17], was used. The O-TPC consists of a time projection chamber with an opto-electronic chain to record the image of each event. The O-TPC was used as target material as well as to detect the outgoing alpha-particles from the  $^{12}\text{C}(\gamma, 3\alpha)$  reaction.

The events recorded in the O-TPC include protons from the  $^{14}\text{N}(\gamma, p)$  reaction, alpha-particles from the  $^{16,18}\text{O}(\gamma, \alpha)$  and the  $^{12}\text{C}(\gamma, 3\alpha)$  reactions and cosmic rays. Nearly all (98%) of the  $^{12}\text{C}$  dissociation events proceed via the  $^{12}\text{C}(\gamma, \alpha_0)^8\text{Be}$  and the subsequent (immediate) decay of the ground state of  $^8\text{Be}$  by two co-linear alpha-particles. As discussed in [17] all events were easily distinguished from the  $^{12}\text{C}(\gamma, 3\alpha)$  events except for the  $^{16}\text{O}(\gamma, \alpha)$  events. The recorded energy and track of the  $^{12}\text{C}$  and  $^{16}\text{O}$  dissociation events are very similar and the events are separated

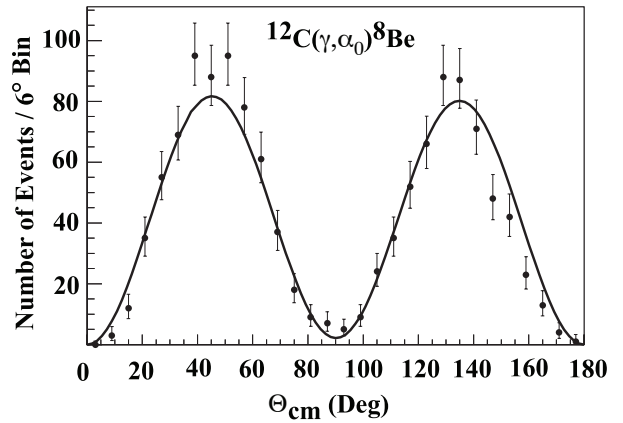


**Fig. 2.** Angular distribution of the  $^{12}\text{C}(\gamma, \alpha_0)^8\text{Be}$  reaction measured at  $E_\gamma = 9.6$  MeV.

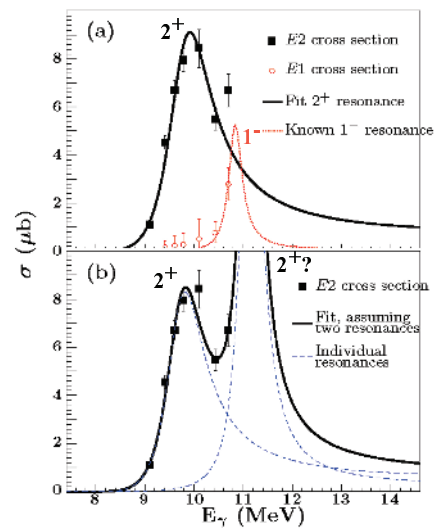


**Fig. 3.** The measured total cross section of the  $^{12}\text{C}(\gamma, 3\alpha)$  reaction (a) separated for  $E1$  and  $E2$  contributions and analyzed using one  $2^+$  state plus the known  $1^-$  state at 10.08 MeV and (b) analyzed with two  $2^+$  states.

using the line shape analysis described in [17]. Each measured time projection signal was fit using the calculated line shapes of the  $^{12}\text{C}(\gamma, \alpha_0)^8\text{Be}$  and  $^{16}\text{O}(\gamma, \alpha)^{12}\text{C}$  events as discussed in [17]. The goodness-of-fit parameters,  $\chi_C^2$  and  $\chi_O^2$  of the predicted line shapes of  $^{12}\text{C}(\gamma, \alpha_0)^8\text{Be}$  and  $^{16}\text{O}(\gamma, \alpha)^{12}\text{C}$  respectively, were used to classify the event as shown in figure 1. Discrimination between  $^{12}\text{C}(\gamma, \alpha_0)^8\text{Be}$  and  $^{16}\text{O}(\gamma, \alpha)^{12}\text{C}$  events (shown in figure 1 for the beam energy of 9.78 MeV) is carried out using the fitted line shape of the time projection signals.

Complete angular distribution of  $^{12}\text{C}(\gamma, \alpha_0)^8\text{Be}$  events were measured at seven energies between 9.1 and 10.7 MeV. The events recorded in the O-TPC (in three dimension) are transformed to the  $(\theta, \phi)$  coordinate system as discussed in [17]. The angular distributions were fit in terms of  $E1$  and  $E2$  amplitudes and their relative phase  $\phi_{12}$  [18]. Since angular information was available for each  $^{12}\text{C}(\gamma, 3\alpha)$  event individually, unbinned maximum likelihood fits were used

to avoid losing information through binning. This also reduced the number of fitting parameters, as the fitting function is normalized to unity. An angular distribution at a gamma-ray beam energy of 9.6 MeV is shown in figure 2. The solid curve is the fitted angular distribution calculated for  $\frac{\sigma(E2)}{\sigma} = 96.75\%$  and  $\phi_{12} = 80.3^\circ$ . For almost all beam energies the angular distributions were dominated by the  $E2$  component.

The total cross section yield curve was deduced from the angular distribution measured at seven different gamma-ray beam energies between 9.1 and 10.7 MeV, as shown in figure 3 with error bars that include both statistical and systematic uncertainties. The systematic uncertainties associated with each measured cross section are dominated by a 5% uncertainty in the gamma-ray beam intensity. In figure 3a we show the separated  $E1$  and  $E2$  cross section components measured at these energies together with the calculated Breit-Wigner resonances with energy-dependent level shifts and widths [19], convoluted with the measured gamma-ray beam energy distribution. Coulomb wave functions were calculated using the continued-fraction expansion technique [20] with  $R_0 = 1.4$  fm. Each Breit-Wigner term includes three free parameters: the partial widths  $\Gamma_\alpha$ ,  $\Gamma_\gamma$  and the resonance energy.

The  $E2$  cross section data allow us to unambiguously identify a  $2^+$  resonance at 10.03(11) MeV with a total width of 800(130) keV and gamma-decay width of 60(10) meV;  $B(E2 : 2_2^+ \rightarrow 0^+) = 0.73(13) e^2\text{fm}^4$  or 0.45 W.u. The measured  $B(E2 : 2_2^+ \rightarrow 0^+)$  is close to prediction of the FMD model ( $0.46 e^2\text{fm}^4$ ) [21], and smaller than predicted in the EFT calculations ( $2(1) e^2\text{fm}^4$ ) [9]. Note that the slight difference between the maximum of the calculated cross section (at 9.8 MeV) and the resonance energy (at 10.03 MeV) is due to the energy-dependent widths used in the fit. The highest energy data point at 10.7 MeV is not consistent with this single resonance hence in order to estimate the error in the measured resonance energy we also analyzed our data including another  $2^+$  that was previously suggested at 11.1 MeV leading to total error of the resonance energy of 110 keV.

### 3 Conclusion

The measured  $2_2^+$  state at 10.03(11) MeV reported in this work lies 2.47(11) MeV above the  $0^+$  Hoyle state, 0.56(3) times the excitation energy of the  $2_1^+$  state of  $^{12}\text{C}$ . We thus conclude that the rotational Hoyle band has a moment of inertia approximately twice as large as the ground state rotational band. Relying on the U(7) model that predicts the ground state rotational band and the Hoyle bands to arise from the same geometrical shape we can conclude that the rms radius of the Hoyle state is  $\sqrt{1.8} \times 2.4 = 3.22(8)$  fm. Our result is close to the prediction of the Fermionic Molecular Dynamic (FMD) model (3.48 fm) [4], but it is considerably larger than predicted by the ab-initio Lattice Effective Field Theory (EFT) (2.4 fm) [8] and smaller than predicted by the "BEC-like" model (3.83 fm) [5]. It is slightly larger than the one extracted (2.89(4) fm) from  $^{12}\text{C}(p, p')$  data [22]. A third  $2^+$  state above 11 MeV cannot be excluded by our data but a further study at higher energy is required to confirm the hint of a third  $2^+$  state observed in this study.

### References

1. F. Hoyle, D.N.F. Dunbar, W.A. Wenzel, W. Whaling, Phys. Rev. **92**, 1095c (1953) in Minutes of the New Mexico Meeting held at Albuquerque, Sept. 2-5.
2. D.M. Brink, Proc. Intern. School of Physics "Enrico Fermi", course 36, Ed. C.Block (Academic Press, 1966)
3. R. Bijker and F. Iachello, Ann. Phys. **298**, 334 (2002)
4. M. Chernykh, H. Feldmeier, T. Neff, P. von Neumann-Cosel, and A. Richter, Phys. Rev. Lett. **98**, 032501 (2007)
5. Y. Funaki, H. Horiuchi, W. von Oertzen, G. Röpke, P. Schuck, A. Tohsaki, and T. Yamada, Phys. Rev. C **80**, 64326 (2009) and references therein.
6. R. Roth, J. Langhammer, A. Calci, S. Binder, and P. Navratil, Phys. Rev. Lett. **107**, 072501 (2011)
7. J.P. Draayer, T. Dytrych, K.D. Launey, D. Langr, A.C. Dreyfuss, and C. Bahri, Proc. Oaxtepec 2012 Conference, Mexico, to be published, J. Phys. CS, 2012.
8. E. Epelbaum, H. Krebs, D. Lee, and Ulf-G. Meissner, Phys. Rev. Lett. **106**, 192501 (2011)
9. E. Epelbaum, H. Krebs, T. Lahde, D. Lee, and Ulf-G. Meissner, arXiv1208.1328 (2012)
10. R. Bijker, A.E.L. Dieperink, and A. Leviatan, Phys. Rev. A **52**, 2786 (1995)
11. R. Bijker, F. Iachello, and A. Leviatan, Ann. Phys. **236**, 69 (1994)
12. Simon Capstick and Nathan Isgur, Phys. Rev. D **34**, 2809 (1986)
13. H.R. Weller, M.W. Ahmed, H. Gao, W. Tornow, Y.K. Wu, M. Gai, and R. Miskimen, Prog. Part. Nucl. Phys. **62**, 257 (2009)
14. C. Sun and Y.K. Wu, Phys. Rev. ST Accel. Beams **14**, 044701 (2011)
15. C. Sun, Y. Wu, G. Rusev, and A. Tonchev, Nucl. Inst. Meth. Phys. Res. A **605**, 312 (2009)
16. C. Sun, Ph.D. thesis Duke University, 2010.
17. M. Gai, M.W. Ahmed, S.C. Stave, W.R. Zimmerman, A. Breskin, B. Bromberger, R. Chechik, V. Dangelndorf, Th. Delbar, R.H. France III, S.S. Henshaw, T.J. Kading, P.P. Martel, J.E.R. McDonald, P.-N. Seo, K. Tittelmeier, H.R. Weller, and A.H. Young, JINST **5**, 12004 (2010)
18. P. Dyer and C. Barnes, Nucl. Phys. A **233**, 495 (1974)
19. A.M. Lane and R.G. Thomas, Rev. Mod. Phys. **30**, 257 (1958)
20. A.R. Barnett, D.H. Feng, J.W. Steed, and L.J.B. Goldfarb, Comput. Phys. Commun. **8**, 377 (1974)
21. T. Neff, private communication, 2012.
22. A.N. Danilov, T.L. Belyaeva, A.S. Demyanova, S.A. Goncharov, and A.A. Ogloblin, Phys. Rev. C **80**, 054603 (2009)